JOINT EUROPEAN TORUS JET

JET–P(93)24

R.C. Wolf, L-G. Eriksson, M. von Hellermann,
R. König, W. Mandl, F Porcelli

Motional Stark Effect Measurements of the Local ICRH Induced Diamagnetism in JET Plasmas

Motional Stark Effect Measurements of the Local ICRH Induced Diamagnetism in JET Plasmas

R.C. Wolf, L-G. Eriksson, M. von Hellermann,
R. König, W. Mandl[1], F Porcelli

JET-Joint Undertaking, Culham Science Centre, OX14 3DB, Abingdon, UK

[1]Max Planck Institut für Plasmaphysik, Garching, Germany.

Preprint of a paper to be submitted for publication in Nuclear Fusion
April 1993

ABSTRACT

Measurements of the toroidal magnetic field inside the JET tokamak plasma by means of the motional Stark effect are reported. In the vicinity of the resonance layer ion-cyclotron-resoance-heating (ICRH) generates a population of energetic ions. For the first time the diamagnetic change in the toroidal magnetic field due to these ICRH fast ions has been measured. A magnetic field decrease up to 4% has been observed. Oscillations of the toroidal magnetic field caused by sawtooth oscillations of the thermal plasma pressure have been resolved. First results of the local β-increase due to ICRH, the diamagnetic current density and the slowing-down time of the fast particles are presented.

1. INTRODUCTION

The potential of the motional Stark effect (MSE), observed on the Balmer-α emission of high energy neutral hydrogen or deuterium beams, as a diagnostic of the local magnetic field inside a tokamak plasma has been pointed out previously [1,2]. A neutral atom moving with a constant velocity $\vec{v}$ in a magnetic field $\vec{B}$ experiences in its rest frame a Lorentz electric field $\vec{E}_L$ induced by its own motion. This electric field gives rise to the splitting and characteristic polarization pattern of the beam emission (BE) lines. Since hydrogen and its isotopes exhibit a linear Stark effect, the BE spectrum of hydrogen is dominated by the motional Stark effect [3] and therefore presents an ideal diagnostic of the local magnetic field. The polarization pattern of the BE spectrum is a direct measure of the magnetic field direction (pitch angle), while the Stark wavelength splitting contains the information about the strength of the magnetic field, which is essentially a measure of the toroidal magnetic field (fig. 2). The fundamental observation is the correlation between the coupled ICRH-power and $|\vec{E}_L|$ which is attributed to the diamagnetic decrease of the toroidal magnetic field (fig. 2). This conclusion is substantiated by oscillations of the measured toroidal magnetic field due to sawtooth oscillations of the thermal plasma pressure.

Up to now the exploitation of the MSE as a magnetic field diagnostic has focused on the polarimetry of the polarization pattern in order to infer the local pitch angle and subsequently the poloidal magnetic field distribution [4,5,6,7]. In contrast, in the study reported here both the pitch angle and the toroidal magnetic field are measured simultaneously. While the complete setup of the diagnostic and the results concerning the poloidal magnetic field are described

elsewhere [3,8], this report concentrates on the application of the MSE as a toroidal magnetic field diagnostic.

The Stark wavelength splitting which is proportional to the Lorentz electric field (for the linear Stark effect) is derived from the fully resolved BE spectrum by means of a multi-Gaussian fit code. On the basis of the detailed knowledge of the atomic physics involved the code restricts the number of free parameters to the minimum required. As a result, the fit procedure accomplishes an accuracy which allows minute changes of the Stark wavelength splitting and subsequently variations of the toroidal magnetic field of the order of 0.5% to be resolved. The Doppler shift of the BE spectrum allows movements of the observation positions and fluctuations of the beam velocity to be ruled out as possible sources of spurious effects. In addition sensitivity considerations show that neither the Shafranov shift nor ICRH current drive contribute significantly to the observed changes of the Stark splitting. Consequently the changes can be solely attributed to changes of the toroidal magnetic field.

The toroidal magnetic field is studied for plasma discharges with additional ICRH. Close to the resonance layer ICRH creates a minority ion population of high energy which heats the thermal plasma mainly through electron collisions, producing pressure gradients which result in a diamagnetic decrease of toroidal magnetic field. The local measurement of the toroidal magnetic field includes information about the distribution of both the thermal pressure and the anisotropic fast-ion pressure. The evolution of the thermal plasma pressure - measured independently - combined with the PION-T code simulation of the fast ion pressure [9] agree within an order of magnitude with the toroidal field changes and indicate that the contribution of the anisotropic pressure from fast particles to the total pressure increases towards the plasma centre. Discrepancies between the measurement and the prediction made by PION-T at the plasma centre are attributed to the limited accuracy of the equilibrium reconstruction and the difficulty in estimating the local fast ion pressure, in particular, at positions close to the ICRH resonance layer. The capability of resolving oscillations of the toroidal magnetic field caused by sawtooth oscillations of the thermal pressure demonstrates the sensitivity of the diagnostic. First results embrace the local β-change due to ICRH, the diamagnetic current density distribution and an estimate of the slowing down time of the fast ions, which are important quantities in the understanding of the heating process.

2. DIAGNOSTIC

The MSE diagnostic at JET makes use of the neutral hydrogen or deuterium heating beams at octant 8 (fig. 3). The neutral beam injector (NBI) consists of eight sub-systems, so called PINIs (positive ion neutral injector). Each PINI delivers up to 1.2 MW of neutral particle power. The energy range of the injected hydrogen isotopes lies in the range of 35 to 70 keV/amu. The neutral beams are viewed via an optical head located at octant 7. A set of four nearly horizontal lines of sight intersects the uppermost PINIs at major radii between 3.0 m and 3.4 m with an inclination of about 60^{o} relative to the beam axis. The optical head consisting of mirror and lens system images the light onto fibres which relay the collected light from the torus hall to the diagnostic area. The ends of the fibres are arranged in a vertical stack which is imaged onto the entrance slit of 1.25 m Czerny-Turner spectrometer. A two dimensional CCD detector records the spectra from the different plasma locations simultaneously. With this technique a minimum exposure time of 50 msec for spectra with 298 channels wavelength resolution has been achieved. In fig. 4 an overview of the whole MSE diagnostic is shown. In order to obtain a "sharp", well defined velocity vector, for the plasma discharges presented here, only two PINIs have been used.

The spectrum in the vicinity of deuterium Balmer-α (6561 Å) during the NBI phase is shown in fig. 5. The complex structure is associated with a combination of plasma deuterium and neutral beam deuterium emission and separates into three main parts: (1) A cold edge feature with an underlying broad "pedestal", which is also present before the neutral beams are switched on, (2) the charge exchange (CX) signal only observed with the beams, emitted primarily at the beam-viewing line intersection and (3) the Doppler shifted beam emission consisting of the motional Stark spectrum of three energy fractions. The energy fractions correspond to the presence of D^+, D_2^+ and D_3^+ in the positive ion source of the NBI. In addition a weak H_α edge line due to a small amount of hydrogen in the plasma can be observed. Similarly, the description above is valid for hydrogen (and tritium). The baseline level of the line radiation is formed by line integrated bremsstrahlung the intensity of which mainly depends on the plasma density and impurity content. In this report the CX and edge emission is only of interest for retrieving the Doppler shift of the BE and detecting how far the CX part reaches into the BE spectrum. More detailed descriptions of the Balmer-α CX and edge spectrum are given in [2,10].

The main advantages of utilizing the Balmer-α emission from high-power, high-energy neutral hydrogen or deuterium heating beams for the MSE are the following:

- The high power and energy, for the typical densities present at JET (central values from 3 to $5 \cdot 10^{19}$ m^{-3}), ensure a reasonable penetration depth which is necessary to provide a strong enough BE from the plasma interior.
- The high energy leads to a considerable Stark splitting which, for the given magnetic fields ($B \approx 3$ T), exceeds the width of the lines of the BE spectrum. Consequently the obtained resolution allows the splitting to be easily observed.
- The Doppler shift which separates the BE spectrally from the CX and edge radiation is a pre-condition for an exact analysis of the Stark splitting and thus should be as large as possible. This, however, is incompatible with the requirement of a good spatial resolution which necessitates viewing angles relative to the neutral beam close to 90°. In this context the high beam energy permits a compromise between the two requirements. In addition the Doppler shift provides important information, such as the exact radial position, its stability and the stability of the beam velocity.
- The measurement volume is localized to the intersection of the line of sight and the neutral beam.
- The emission is in the visible, thus diagnostic components, such as viewing optics and spectrometers are readily available.

The measured Balmer-α spectrum (fig. 5) is analysed by means of a least square fit code which approximates the spectrum by a superposition of Gaussians. Making use of all the physical relationships the number of free parameters is restricted to the absolute minimum. Hence the fit code obtains an unambiguous result for a spectrum which otherwise would be too complicated to be analysed. One of the most precise parameters determined by the fit code is the Stark wavelength splitting from which the toroidal magnetic field is inferred. Since only wavelength information is involved, no absolute intensity calibration is required and also a relative calibration only needs to ensure that the detector response is linear. The absolute error of the Stark splitting is equal to the error of the spectrometer dispersion which can be determined within ±0.2%. Consequently the uncertainty of a change of the Stark splitting, which is a measure of the diamagnetic change of the toroidal magnetic field, is below the resolution of the

MSE diagnostic (changes of the Stark splitting of the order of 0.5% have been resolved).

3. DEDUCTION OF THE TOROIDAL MAGNETIC FIELD

The local toroidal magnetic field is deduced from the measurement of the Stark wavelength splitting of the BE spectrum. For the linear Stark effect the splitting is directly proportional to the strength of the Lorentz electric field

$$E_L = \frac{2}{3}\frac{hc}{ea_0}\frac{\Delta\lambda}{\lambda_0^2}, \qquad (1)$$

where h is the Planck constant, c the velocity of light, e the electron charge, a_0 the Bohr radius, λ_0 the Balmer-α wavelength and $\Delta\lambda$ the Stark wavelength splitting. Expressed in terms of the magnetic field and the beam velocity, E_L is given by

$$E_L = |\vec{v}|\sqrt{B_{pol}^2 + B_{tor}^2 - \left(\hat{v}_{pol}\, B_{pol} + \hat{v}_{tor}\, B_{tor}\right)^2}. \qquad (2)$$

where B_{pol}, B_{tor} and $\hat{v}_{pol}$, $\hat{v}_{tor}$ are the poloidal, toroidal components of the magnetic field and the unit vector $\vec{v}/|\vec{v}|$ of the beam velocity respectively. For a beam which is injected normal to the magnetic field ($\hat{v}_{pol} = \hat{v}_{tor} = 0$) E_L is simply proportional to the total magnetic field. In the JET neutral beam geometry the normal and the toroidal velocity components generally form the dominant parts (see figs. 3 and 4). From eqn. (2) it becomes already clear that, since B_{pol} for the discharges considered and the radial range covered by the MSE diagnostic is at least a factor of 6.5 smaller than B_{tor}, B_{pol} forms only a minor contribution to the total magnetic field and hence to E_L. In particular, uncertainties of B_{pol} do not introduce significant errors into the evaluation of the toroidal magnetic field from the Lorentz electric field. For instance the neglect of the effect of the Shafranov shift on B_{pol} leads to a maximum error of 0.5% in the derived B_{tor}, as will be shown later. For that reason B_{pol} is taken from the equilibrium code IDENTC [11] without being concerned about the accuracy of the given poloidal field values. In fig. 6 the radial B_{tor}-profile deduced from the Lorentz field strength is compared with the profile, as given by IDENTC, and the vacuum B_{tor}, calculated from the toroidal field coil current. The deviations of the measured values from the IDENTC result are less than 3%. This can be attributed to either a radial mis-match < 10 cm between IDENTC and the measurement or a 3% error

of the beam velocity. The error of the spectrometer dispersion (±0.2%) is too small to explain the deviations. However, the important quantity detecting the plasma diamagnetism is the relative sensitivity to toroidal field changes. Only limited by statistical noise, it lies between 0.1% and 1% and depends on the intensity of the beam emission and thus on the plasma density and penetration depth of the beam.

In the following sections possible sources of spurious effects will be discussed which could lead to changes of the Lorentz electric field not correlated with the diamagnetic behaviour of the toroidal magnetic field. According to eqn. (2) there are five such possibilities:

- Because of the 1/R dependence (R: major radius) of the toroidal magnetic field the slightest radial movement of the observation position shows up in a change of E_L.
- Fluctuations of the beam energy (E_L is proportional to the beam velocity $|\vec{v}|$) produce fluctuations of E_L.
- ICRH increases the plasma pressure which first of all is the reason for the diamagnetism, but also is a cause for a displacement of the flux surfaces (Shafranov shift). If not sufficiently detected by the equilibrium reconstruction and hence not considered in the calculation of B_{tor}, it could lead to an apparent change of B_{tor}.
- The influence of ICRH current drive on the current distribution and hence B_{pol} may be large enough to give rise to significant changes of E_L.
- The JET plasma generally is paramagnetic. In the presence of a substantial Shafranov shift the paramagnetic correction to the vacuum toroidal field also moves which causes a change of the locally observed toroidal magnetic field.

The major radius of the observation position and hence also its stability is deduced from the Doppler shift of the beam emission relative to the cold edge feature. In this context a small but detectable variation of the Doppler shift has been observed (fig. 7) which can be attributed to either a fluctuation of the beam velocity or a radial movement of the observation positions. It should be noted that the variations for different radial channels evolve coherently, as expected, since the Doppler shift does not depend on any local plasma parameter which could produce an independent behaviour of the individual channels. The amplitude of the variations of less than 0.1 Å is equivalent to a radial movement of the observation positions relative to the neutral beam of $\Delta R < 3$ **mm** or a

relative change of the beam velocity of $\Delta v/v < 0.2\%$. Since, for both cases, the subsequent relative change of the Lorentz electric field lies below 0.2%, the interpretation of the measurement in terms of a toroidal magnetic field effect is not affected. Besides, the evolution of the Lorentz electric field is correlated with the ICRH wave form, whereas the Doppler shift changes are not.

The typical Shafranov shift at JET due to ICRH is about 5 to 10 cm (fig. 8). In order to get an upper limit for the influence on the Lorentz electric field, it is assumed that the complete poloidal field profile simply moves radially and that in addition both beam and observation positions are lying in the magnetic midplane ($\hat{v}_{pol} = 0$). The local change of the Lorentz electric field due to the Shafranov shift then becomes

$$\frac{\delta E_L}{E_L} \leq \frac{B_{pol}\,\delta B_{pol}}{(E_L/v)^2}. \qquad (3)$$

For the plasma discharges presented in this report, it follows

$$\frac{\delta B_{pol}}{\delta R} \leq 1.2\ T/m,\ \delta R \leq 0.07\ m,\ B_{pol} \leq 0.4\ T, \quad \Rightarrow \quad \frac{dE_L}{E_L} \leq 0.5\%\ ,,$$

which is generally small enough to be neglected. This means that even if the Shafranov shift is not recognised by the equilibrium code, which is obviously not the case (fig. 8), it does not affect E_L within the resolution of the measurement. Certainly errors made by the equilibrium reconstruction of the Shafranov shift can be ignored.

According to theoretical investigations [12] the ICRH minority ions can carry a toroidal current density due to the toroidal component of their drift motion which scales as $j_{\parallel,fast} \approx 0.5\, e\, n_{fast}\, v_{fast} \sqrt{\delta / R}$, where n_{fast} is the fast ion density, v_{fast} the root-mean-square fast particle velocity and $\delta \approx (2\, q\, v_{fast}/\Omega R)^{2/3} R$ the characteristic width of a trapped particle orbit near the plasma centre (q: safety factor, Ω: cyclotron frequency of minority ions, and R: major radius). This current is mainly concentrated within a distance $\approx \delta$ from the magnetic axis. It is interesting to note that, for 10 MW ICRH power in JET, the total fast ion current can be as big as 0.3 MA. This current is partly compensated by an electron back current such that the actual ICRH driven current is $I_{RF} \approx \pi \delta^2\, j_{\parallel,fast}\, (1 - Z_{eff}/Z_{fast})$, with Z_{eff} the effective ion charge and Z_{fast} the minority ion charge. The related

poloidal field change, however, gives rise to a change in the magnitude of the total magnetic field not larger than $\Delta B / B \approx 0.5\ (\mu_0 j_{\parallel,fast}\ \delta/B)^2 \approx 10^{-4}$, which is indeed negligible compared with the observed Lorentz field variations. Thus it can be concluded that the observed changes of the Lorentz electric field can be attributed solely to the toroidal magnetic field.

There are now two toroidal field effects which have to be considered. The diamagnetic decrease of B_{tor} due to a pressure rise and a variation of the paramagnetic correction of the vacuum toroidal field due to a change of the toroidal current distribution. JET plasmas with ohmic heating are generally paramagnetic, so that the plasma toroidal magnetic field is larger than the vacuum field. In the plasma centre the paramagnetic correction amounts to about 5% and at the edge goes to zero. When additional heating is applied the plasma and fast ion pressure are sufficient that in the highest performance plasmas there is a small net diamagnetic contribution. The Shafranov shift now also moves the paramagnetic correction which locally leads to a change in the toroidal magnetic field. An estimate of this effect is obtained by shifting the paramagnetic correction radially according to the Shafranov shift, which is illustrated in fig. 9. For observation positions close to the magnetic axis the resulting change of the local toroidal field **(< 0.2%)** can be neglected. For the position at R = 3.42 m the effect is already large enough to be observed (about 40% of the measured change). However, for the positions with radii larger than 3.05 m the shift of the paramagnetic correction causes a field rise which is opposite to the observed drop. This means that, if a decrease of the toroidal magnetic field is observed while the plasma moves towards larger radii, it certainly can be attributed to the plasma diamagnetism. Consequently the actual toroidal field decrease at 3.42 m is larger than the measured value. In particular very small toroidal field variations, such as sawtooth oscillations, are caused by the changing plasma pressure and not by a movement of the magnetic axis, if a toroidal field drop is associated with a pressure rise.

The correlation of the toroidal magnetic field inferred from the MSE with the poloidal flux measured by diamagnetic loops (fig. 10) gives further evidence that the observed effects are associated with the plasma diamagnetism. A quantitative comparison of the two diagnostics, however, is not very feasible, since the diamagnetic loop detects the flux through the total cross-section of the tokamak, whereas the MSE measurement only covers a small fraction of that area.

4. ICRH-INDUCED DIAMAGNETISM

The toroidal magnetic field is directly evaluated from the measured Lorentz electric field using eqn. (2). Fig. 11 shows the toroidal field evolution so obtained in comparison with the radio frequency (RF) wave form, for two discharges where the ICRH-power was substantially different. Looking back to fig. 2, since the relative changes of B_{tor} and E_L are equal, it is seen that the Shafranov shift has no influence on the interpretation of the Lorentz field decrease as purely a toroidal field effect. In fig. 12 the radial B_{tor}-profiles for the two discharges before and after the onset of ICRH are displayed. In both cases the maximum drop of the toroidal magnetic field is located at the measurement position closest to the RF resonance layer. The shaded regions indicate the B_{tor}-dependent movement of the resonance layer. It should be noted that the decrease of B_{tor} is correlated with the RF wave form, while the strength and radial extent of the decrease rises with the coupled ICRH-power. In case of pulse no. 27019 the only detectable B_{tor}-change (> 0.5%) is confined to a single observation position.

As already indicated in the previous sections, the explanation for such a toroidal field decrease is the diamagnetism of the plasma caused by an increasing kinetic pressure in the central regions of the plasma. In the case of a RF heated plasma two contributions to the pressure have to be considered: (1) The RF wave directly couples into the gyration of the minority ions and thus, by only increasing the pressure perpendicular to the magnetic field substantially, creates an anisotropic pressure distribution. (2) The energy of these fast ions is transferred to the thermal plasma mainly through electron collisions, resulting in a rise of the isotropic thermal pressure. Hence the pressure balance between the period of the discharge before and during ICRH becomes (see appendix):

$$\underset{\text{before}}{p_{1,th} + \frac{B_{1,tor}^2}{2\,\mu_0}} = \underset{\text{during ICRH}}{p_{2,th} + p_{\perp,fast} + \frac{B_{2,tor}^2}{2\,\mu_0}}. \qquad (4)$$

From the change of the thermal pressure ($p_{2,th}$-$p_{1,th}$) and the additional perpendicular fast-ion pressure ($p_{\perp,fast}$) the expected decrease of the toroidal magnetic field due to ICRH now can be evaluated. It has to be emphasized that only field changes relative to an initial value, which here is the measured toroidal field before the ICRH phase, are calculated. Thus neither absolute errors

of the measurement nor the effect of 2 MW of "diagnostic" beams, nor paramagnetic corrections have to be taken into account, as they all are constant off-sets which cancel out, if only diamagnetic field changes are considered.

The thermal pressure is deduced from the electron temperature T_e and density n_e:

$$p_{th} = 2\, n_e\, kT_e. \qquad (5)$$

The electron temperature is provided by the electron cyclotron emission measurement [13], the electron density by the far infrared interferometer [14]. Since no profile data for ion densities n_i and temperature T_i are available for the discharge considered, $n_e = n_i$ and $T_e = T_i$ is assumed. The single point measurement at the plasma centre (3.1 m) of the main impurity densities and temperatures by charge exchange recombination spectroscopy [15] indicates that T_e is only marginally higher than T_i (10% to 20%), whereas a substantial impurity influx is observed. Taking the ion densities into account, $2\, n_e\, kT_e$ over-estimates the pressure by 10% to 30%.

The fast-ion pressure is modelled by the PION-T code, which calculates the ICRH power deposition and the ion velocity distribution self-consistently [9]. All input data of the code such as T_e and n_e, except the minority concentration which is assumed to be 5%, are taken from experimental data. The simulated energy content though, is not particularly sensitive to the minority concentration. The effects of the finite orbit widths of the trapped high energy ions are taken into account in the latest version of PION-T, which is necessary to treat cases properly, where very energetic ions are present and consequently the orbit widths become larger than the power deposition profile. Fig. 13 shows the calculated flux-surface-averaged profile of the perpendicular fast-ion pressure. Since RF-induced diffusion is not considered in PION-T, the accuracy at the plasma centre is limited which is reflected in the abrupt drop of $p_{\perp,fast}$ towards the magnetic axis. More realistically would be a less abrupt drop of the profile between the resonance layer and the magnetic axis. At larger radii, however, the neglect of RF-induced diffusion is of less importance. Additional uncertainties are introduced by errors in the flux surface mapping from the equilibrium reconstruction (IDENTC) used by the PION-T code to evaluate the flux-surface-averaged quantities and, in particular, the resonance location, which relies on the local toroidal field values from IDENTC. As a result the calculated pressure profile has to be shifted, in order to match the peak of the profile with the maximum of the MSE B_{tor}-

measurement. Without this adjustment the maximum of the MSE measurement coincides with the minimum of the calculated $p_{\perp,fast}$ at the magnetic axis.

The time evolution of the different pressure components is shown in fig. 14. Obviously the parallel fast-ion pressure can be neglected against both the perpendicular fast-ion pressure and the thermal pressure. The decrease of the perpendicular fast-ion pressure after reaching an initial peak mainly has its origin in the rising density and the subsequent decrease of the slowing down time of the fast ions ($\tau_s \propto T_e^{3/2}/n_e$).

The simulation of the ICRH-induced diamagnetism of the plasma for the different radial positions and its comparison with the measurement is displayed in fig. 15. The independent contributions to the total toroidal field change are plotted separately. It is seen that the amplitude of the B_{tor}-decrease generally is well reproduced. The increasing noise of the measured B_{tor} in the course of the RF pulse originates from the rising electron density which results in an enhanced beam stopping. At 3.42 m the thermal pressure is sufficient to explain the observed B_{tor}-change. The deviation between the measurement and the simulation can be explained by the neglect of both the plasma impurities in the evaluation of p_{th} and the effect of the Shafranov shift on the paramagnetic correction. Approaching the resonance layer the fast-ion part becomes increasingly dominating until at 2.99 m it is the major contribution to the diamagnetic effect. This is reflected in the very strong gradient of $p_{\perp,fast}$, while the gradient of the thermal pressure is negligible between 2.99 m and 3. 42 m (the p_{th}-profile is even slightly hollow in this region). At the position closest to the resonance layer the simulation is not satisfactory. The measured decrease of B_{tor} is much bigger than the simulated evolution, except for the initial peak which, however, is not seen on the measurement. This disagreement at R = 2.99 m is most likely due to problems with the equilibrium reconstruction and, in particular, the determination of the resonance location. In the simulation the flux surface at 2.99 m intersects the cyclotron resonance at the beginning of the heating phase and then drifts out to the resonance. The result is a rapid rise followed by a sharp drop of the fast-ion pressure. On the other hand, the measured pressure shows a slow rise (the measured toroidal magnetic field a slow decrease) in the initial phase of the heating. This behaviour is qualitatively different from that of the toroidal field measured at the other positions, indicating that the flux surface at 2.99 m does not intersect the resonance at the

beginning, but drifts into it later. Owing to the small volume in the centre the discrepancy discussed above can only have a minor effect on the global fast-ion energy content. Thus one should not emphasize this discrepancy too much. Nevertheless the comparison of measurement and simulation in the centre has been included for completeness and to illustrate the problem.

Comparing the B_{tor}-measurement with the contribution of the thermal pressure change only, shows that at the positions close to the resonance layer the thermal pressure cannot account for the observed B_{tor}-decrease, which indicates that fast ions are actually involved. As discussed previously impurities and possible differences between the electron and ion temperature have been neglected in p_{th}. Consequently the thermal pressure and its change due to ICRH used here are an upper limit. As a result the deduced contribution of the thermal plasma (fig. 15) to the diamagnetic decrease of B_{tor} represents an upper limit which suggests that the contribution of the fast ions is even higher.

The more detailed features are best observed on the two intermediate channels where, on the one hand the B_{tor}-changes are already substantial enough to reveal more detailed information, and on the other hand the deterioration of the signal quality due to the increasing beam stopping is not too high. Comparing the measured with the simulated B_{tor} at these radii (3.19 m and 3.09 m) it is seen that the measured signal also shows the initial peaking of the diamagnetic decrease, which in the previous discussion has been attributed to the change of the slowing down time of the fast ions. In particular at the beginning of the ICRH phase the measured B_{tor} follows small fluctuations of the simulated signal. Looking at the individual contributions to the simulated B_{tor}, only the electron temperature exhibits significant oscillations (sawtooth oscillations with $\delta T_e / T_e \approx 30\%$). Direct comparison of T_e with the measured B_{tor} brings out this correlation (fig. 16). The fact that not only the global effect of ICRH on the measured toroidal field can be reproduced by calculating the field changes from n_e, T_e and $p_{\perp,fast}$, but also small effects, such as the variation of $p_{\perp,fast}$ and sawtooth oscillations of T_e, is further evidence that the observed B_{tor}-changes can be attributed to the diamagnetism of the plasma.

5. APPLICATIONS

In this paragraph applications of the measurement of the toroidal magnetic field are described. In particular quantities related to the diamagnetism of the plasma

which have not been directly accessible previously because of there local character are presented.

Diamagnetic Current Density

Associated with the pressure gradient of the plasma is the diamagnetic current, which produces a magnetic field opposite to the externally-applied field. In the cylindrical approximation the diamagnetic current density is equal to the poloidal current density which is given by

$$j_{diam} = j_{pol} = -\frac{1}{\mu_0}\frac{dB_{tor}}{dr}. \qquad (6)$$

Since the measurement positions are fairly close to the plasma centre where the elongation of the JET plasma is small, the cylindrical approximation gives a reasonable estimate of j_{diam}. For the calculation of j_{diam}, however, because of its smallness, any radial dependence of B_{tor}, which is not related to the diamagnetism, has to be eliminated. This is achieved by subtracting the diamagnetic change ΔB_{tor} from the radial average. Considering dr = dR, the diamagnetic current density becomes

$$j_{diam} = -\frac{1}{\mu_0}\frac{d(\Delta B_{tor})}{dR}. \qquad (7)$$

The diamagnetic change of the toroidal magnetic field and the inferred diamagnetic current density are plotted in fig. 17. In order to get a smooth fit to the four data points, from which $d(\Delta B_{tor})/dR$ is calculated, $\Delta B_{tor} = 0$ and $d(\Delta B_{tor})/dR = 0$ has been assumed at the plasma edge. The maximum j_{diam} has about 5% of the strength of the maximum toroidal current density (1.5 MA/m^2).

β-Increase due to ICRH

The local β-increase which is a measure of the increase of the plasma energy content is given by

$$\Delta\beta = -2\frac{\Delta B_{tor}}{B_{tor}}, \qquad \beta << 1. \qquad (8)$$

From the measured ΔB_{tor}, $\Delta\beta$ can be evaluated (fig. 18). Although the highest volume average β-value achieved for a JET plasma is 6% [16], the central β can be significantly higher. In the case presented here the maximum β-change due to ICRH is already 7% for a discharge with only a moderate additional ICRH-power of 9 MW.

Slowing Down Time of Fast Ions

The slowing down time of the fast minority ions depends on the electron temperature (T_e) and density (n_e) of the plasma [17,18]:

$$\tau_s[\mathrm{sec}] = 2.0\,\frac{A}{Z^2}\,\frac{T_e^{3/2}[\mathrm{keV}]}{n_e\left[10^{19}\,\mathrm{m}^{-3}\right]\ln\Lambda}, \qquad (9)$$

where A is the mass number and Z the atomic number of the minority ions. Due to the high energy of the minority ions the slowing down process is governed by ion-electron collisions. For the density and temperature range of JET (1-10 keV, 10^{19}-10^{20} m^{-3}) the value of the Coulomb logarithm for ion-electron collisions is approximately 17. The slowing down time can be estimated from the evolution of the toroidal field at the end of the RF pulse. After the ICRH-power is switched off the decay of the fast-ion population causes the toroidal magnetic field to rise until it approximately reaches its initial value (fig. 15). The time constant of this rise is a direct measure of the slowing down time. Provided electron density and temperature and subsequently τ_s change slower than B_{tor} increases, τ_s is given by

$$\tau_s = \frac{B_{tor,0} - B_{tor}}{dB_{tor}/dt}, \qquad (10)$$

where $B_{tor,0}$ is the initial value before (or after) the ICRH period. The comparison of τ_s deduced from the 2.99 m position, where the fast ions dominate the signal, with the value deduced from electron density and temperature gives reasonable agreement:

B_{tor} measurement:	τ_s = (280 ± 101) msec
From n_e and T_e:	τ_s = 366 msec

Remaining deviations may be due to the assumption that τ_s changes on a much slower time scale than B_{tor} which, in the case presented, is only marginally satisfied:

$$\left(dB_{tor} / dt\right) / \left(B_{tor,0} - B_{tor}\right) \approx 2 \left(d\tau_s / dt\right) / \tau_s .$$

In the deduction of the slowing down time, field diffusion effects have not been considered. If they are significant, τ_s has to be regarded as an upper limit for the slowing down time of the fast particles.

6. SUMMARY AND CONCLUSIONS

Employing the motional Stark effect on the hydrogenic heating beams, a high resolution measurement of the internal toroidal magnetic field distribution has been achieved. The main features of the diagnostic and analysis procedure were described, highlighting the measurement accuracy which was obtained.

Changes of the toroidal magnetic field strength have been observed, which are correlated with the ICRH-induced increase of the plasma pressure. Hereby the additional information given by the beam emission spectrum, such as the Doppler shift, permits the elimination of spurious effects. The simulation of the plasma diamagnetism inferred from the independent measurement of the thermal pressure and the code simulation of the anisotropic fast-ion pressure, although not completely reproducing the measurement, clearly shows that both thermal and anisotropic pressure contributions are involved. In particular at the plasma centre the thermal pressure cannot account for the observed toroidal field decrease, indicating a substantial contribution from fast minority ions. The sensitivity of the diagnostic has been demonstrated by resolving sawtooth oscillations of the toroidal magnetic field, due to the redistribution of the thermal pressure in the plasma core. In addition, this is corroborating evidence that the measured toroidal field variations actually can be attributed to changes of the plasma pressure. The sensitivity, however, is not high enough to address the question whether also sawtooth oscillations of the fast ions are involved. Certainly, in the case presented the sawtooth oscillations of the thermal plasma form the dominating part.

The applications of the toroidal magnetic field measurement embrace the determination of diamagnetic current distribution, the β-increase due to ICRH, and the slowing down time of the fast ions. Even for a plasma with moderate

heating power the local β-increase reaches 7%, already lying above the limit of the volume-average β. In the future the MSE diagnostic will cover more of the poloidal cross-section which allows global quantities, such as the fast-ion energy content, to be deduced.

ACKNOWLEDGEMENTS

We wish to thank all those who provided data incorporated in this paper, in particular J. O'Rourke and the members of the electron temperature group. We gratefully acknowledge the continuous support and encouragement of P. R. Thomas and discussions with P. Breger and L. Horton. We also wish to thank G. Decker for his early work on the Stark effect diagnostic at JET.

This publication forms part of a doctoral thesis by R. C. Wolf at the University of Düsseldorf, FRG.

APPENDIX

Here an estimate of the error is presented, which is introduced into the pressure balance equation

$$p + \frac{B^2}{2\mu_0} = \text{const.} \qquad \text{(A.1)}$$

if the isotropic pressure p is substituted by the perpendicular component $p_\perp$ of an anisotropic pressure distribution. In an anisotropic plasma the scalar pressure in $\vec{j} \times \vec{B} = \nabla p$ has to be replaced by the pressure tensor

$$\vec{\vec{P}} = p_\perp \vec{\vec{I}} + \left(p_\parallel - p_\perp\right) \vec{e}_\parallel \vec{e}_\parallel, \qquad \text{(A.2)}$$

where $p_\parallel$ and $p_\perp$ are the pressure components parallel and perpendicular to the magnetic field respectively, $\vec{\vec{I}}$ is the unity tensor and $\vec{e}_\parallel$ is the unit vector in the field direction. $\vec{e}_\parallel \vec{e}_\parallel$ is the so called dyadic product. Consequently

$$\vec{j} \times \vec{B} = \nabla \cdot \vec{\vec{P}}, \qquad \text{(A.3)}$$

where

$$\begin{aligned} \nabla \cdot \vec{\vec{P}} = {} & \nabla p_\perp \\ & + \left(\nabla\left(p_\parallel - p_\perp\right) \cdot \vec{e}_\parallel\right) \vec{e}_\parallel \qquad \text{(i)} \\ & + \left(p_\parallel - p_\perp\right)\left(\nabla \cdot \vec{e}_\parallel\right) \vec{e}_\parallel \qquad \text{(ii)} \\ & + \left(p_\parallel - p_\perp\right)\left(\vec{e}_\parallel \cdot \nabla\right) \vec{e}_\parallel \qquad \text{(iii).} \end{aligned} \qquad \text{(A.4)}$$

As the plasma positions where the anisotropic pressure is of the order of the thermal pressure are close to the magnetic axis, the cylindrical approximation will be used in the following. In cylindrical coordinates, where only the radial derivatives do not vanish, terms (i) and (ii) are zero, while the radial component of (iii) becomes

$$\left[\left(\vec{e}_\parallel \cdot \nabla\right) \vec{e}_\parallel\right]_r = -\frac{B_{pol}^2}{B^2 r}, \qquad \text{(A.5)}$$

and consequently

$$\left[\vec{j} \times \vec{B}\right]_r = \frac{dp_\perp}{dr} - \left(p_\parallel - p_\perp\right)\frac{B_{pol}^2}{B^2 r}. \qquad \text{(A.6)}$$

This means that, in the case that the second term of eqn. (A.6) can be neglected, the isotropic pressure in eqn. (A.1) can be replaced by $p_\perp$. Assuming a parabolic pressure profile

$$p_\perp = p_{\perp,0}\left(1 - \alpha_p\left(\frac{r}{a}\right)^2\right), \qquad \alpha_p = \frac{1}{2}\frac{a^2}{p_{\perp,0}}\frac{d^2 p_\perp}{dr^2}, \tag{A.7}$$

where a is the minor radius of the plasma, and $B \approx B_{tor}$, the ratio of the two terms of eqn. (A.6) becomes

$$\left|\frac{\left(p_\perp - p_\parallel\right) r/(q\,R)^2}{dp_\perp/dr}\right| = \frac{\left(p_\perp - p_\parallel\right)}{2\,p_{\perp,0}\,\alpha_p}\frac{\varepsilon^2}{q^2}, \qquad \varepsilon = \frac{a}{R}. \tag{A.8}$$

Considering that $p_\perp - p_\parallel \le p_\perp \le p_{\perp,0}$ and $1 \approx q_0 \le q$, an upper limit of this ratio is obtained:

$$\left|\frac{\left(p_\perp - p_\parallel\right) r/(q\,R)^2}{dp_\perp/dr}\right| \le \frac{\varepsilon^2}{2\,\alpha_p}. \tag{A.9}$$

Since the pressure profile in the presence of fast ions is sufficiently steep in the central regions of the plasma ($\alpha_p > 1$), the error made by neglecting the second term in eqn. (A.6) is of the order $\varepsilon^2/2$ which for JET is about 5% (the aspect ratio ε of JET is about 30%).

REFERENCES

[1] R. P. Seraydarian, K. H. Burrell, R. J. Groebner
Rev. Sci. Instr. **59** (1988) 1530

[2] A. Boileau, M. von Hellermann, W. Mandl, H. P. Summers, H. Weisen, A. Zinoviev
J. Phys. B: At. Mol. Opt. Phys. **22** (1989) L145

[3] W. Mandl, R. C. Wolf, M. G. von Hellermann, H. P. Summers
submitted for publication (accepted) in Plasma Phys. Contr. Fus. (1993)

[4] F. M. Levinton, R. J. Fonck, G. M. Gammel, R. Kaita, W. Kugel, E. T. Powell, D. W. Roberts
Phys. Rev. Lett **63** (1989) 2060

[5] D. Wróblewski, K. H. Burrell, L. L. Lao, P. Politzer, W. P. West
Rev. Sci. Instrum. **61** (1990) 3552

[6] F. M. Levinton
Rev. Sci. Instr. **63** (1992) 5157

[7] D. Wróblewski, L. L. Lao
Rev. Sci. Instr. **63** (1992) 5140

[8] R. C. Wolf, J. O'Rourke, A. W. Edwards, M. von Hellermann
submitted for publication (accepted) in Nucl. Fus. Let. (1993)

[9] L.-G. Eriksson, U. Willen, T. Hellsten, Proc. Course and Workshop on Theory of Fusion Plasmas, Varenna (1990), 421

[10] W. Mandl, M von Hellermann, P. D. Morgan, H. P. Summers, H. Weisen, M. Olsson, P. van Belle, T. Elevant, G. Sadler
Proc. 17th Eur. Conf. on Controlled Fusion and Plasma Physics, Amsterdam (1990), Part IV, 1496

[11] M. Brusati, J. P. Christiansen, J. G. Cordey, K. Jarrett, E. Lazzaro, R. T. Ross
Comp. Phys. Rep. **1** (1984) 345 (*IDENTC is an updated version of IDENTB which is described in this reference*).

[12] L.-G. Eriksson, H. L. Berk, F. Porcelli, R. Stankiewicz
Proc. 19th Eur. Conf. on Controlled Fusion and Plasma Physics, Innsbruck (1992), Part II, 1469

[13] A. E. Costley
Proc. Course and Workshop on Basic and Advanced Diagnostic Techniques for Fusion Plasmas, Varenna (1991), 223

[14] G. Braithwaite, N. Gottardi, G. Magyar, J. O'Rourke, J. Ryan, D. Véron
Rev. Sci. Instr. **60** (1989) 2825

[15] M. G. von Hellermann, W. Mandl, H. P. Summers, H. Weisen, A. Boileau, P. D. Morgan, H. Morsi, R. König, M. F. Stamp, R. Wolf
Rev. Sci. Instr. **61** (1990) 3479

[16] D. Stork, et al.
Proc. 19th Eur. Conf. on Controlled Fusion and Plasma Physics, Innsbruck (1992), Part I, 339

[17] T. H. Stix
Nuclear Fusion **15** (1975) 737

[18] J. A. Wesson
Tokamaks, Clarendon Press, Oxford (1987)

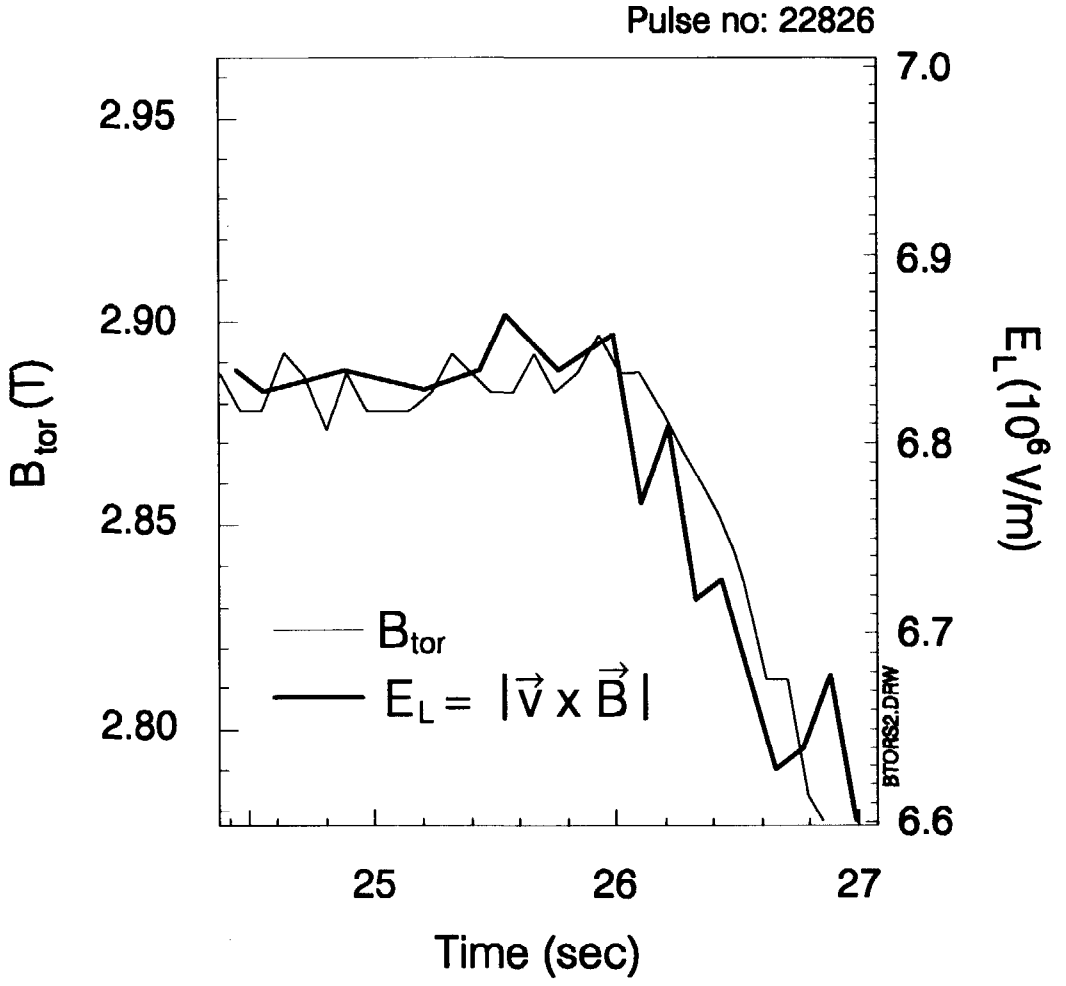

Fig. 1. Toroidal field ramp experiment demonstrating the capability for a high resolution measurement of the local toroidal magnetic field (B_{tor}).

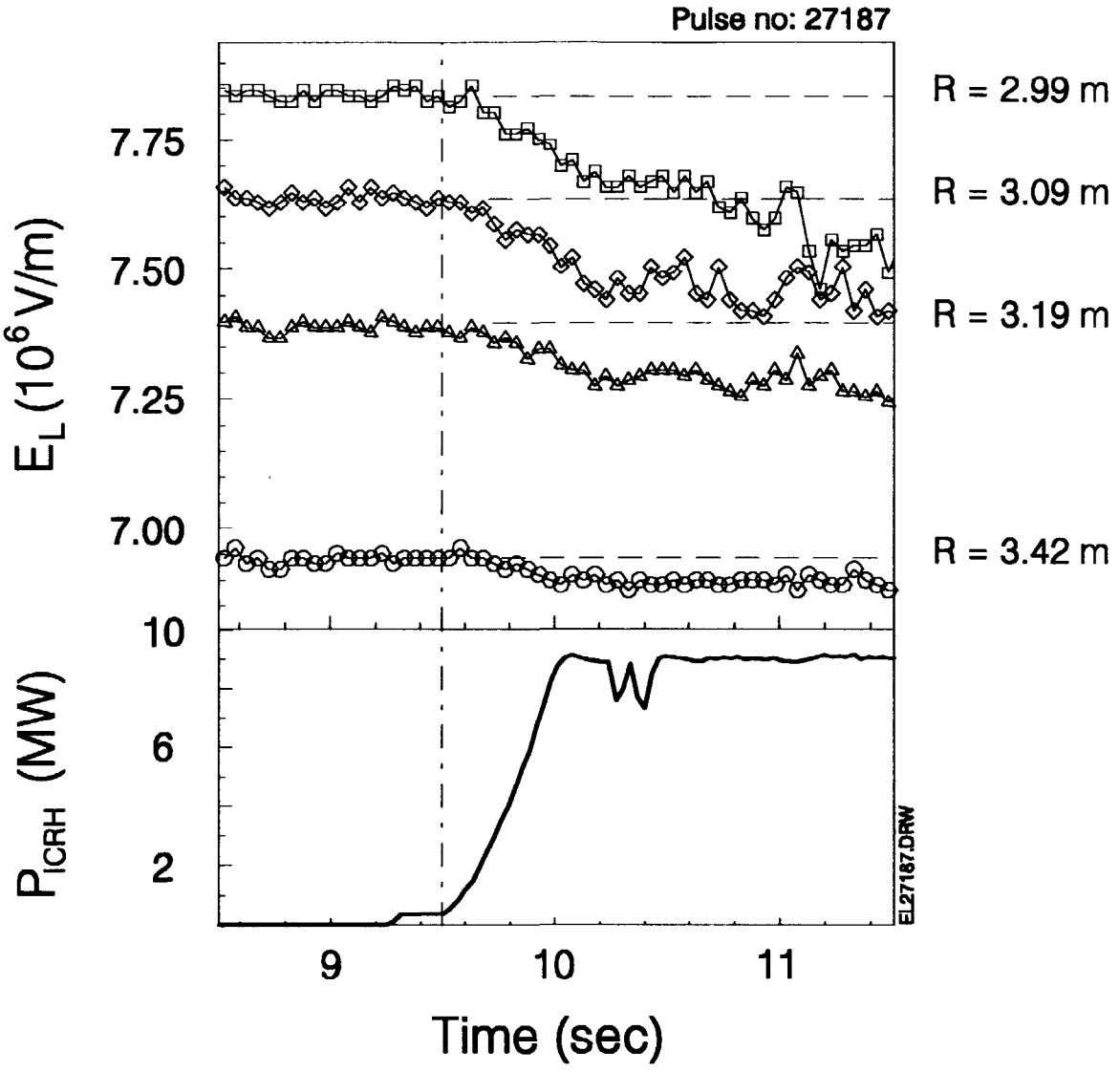

Fig. 2. Correlation between the measured strength of the Lorentz electric field E_L and the total coupled ICRH-power P_{ICRH} at the different observation positions (R: major radius).

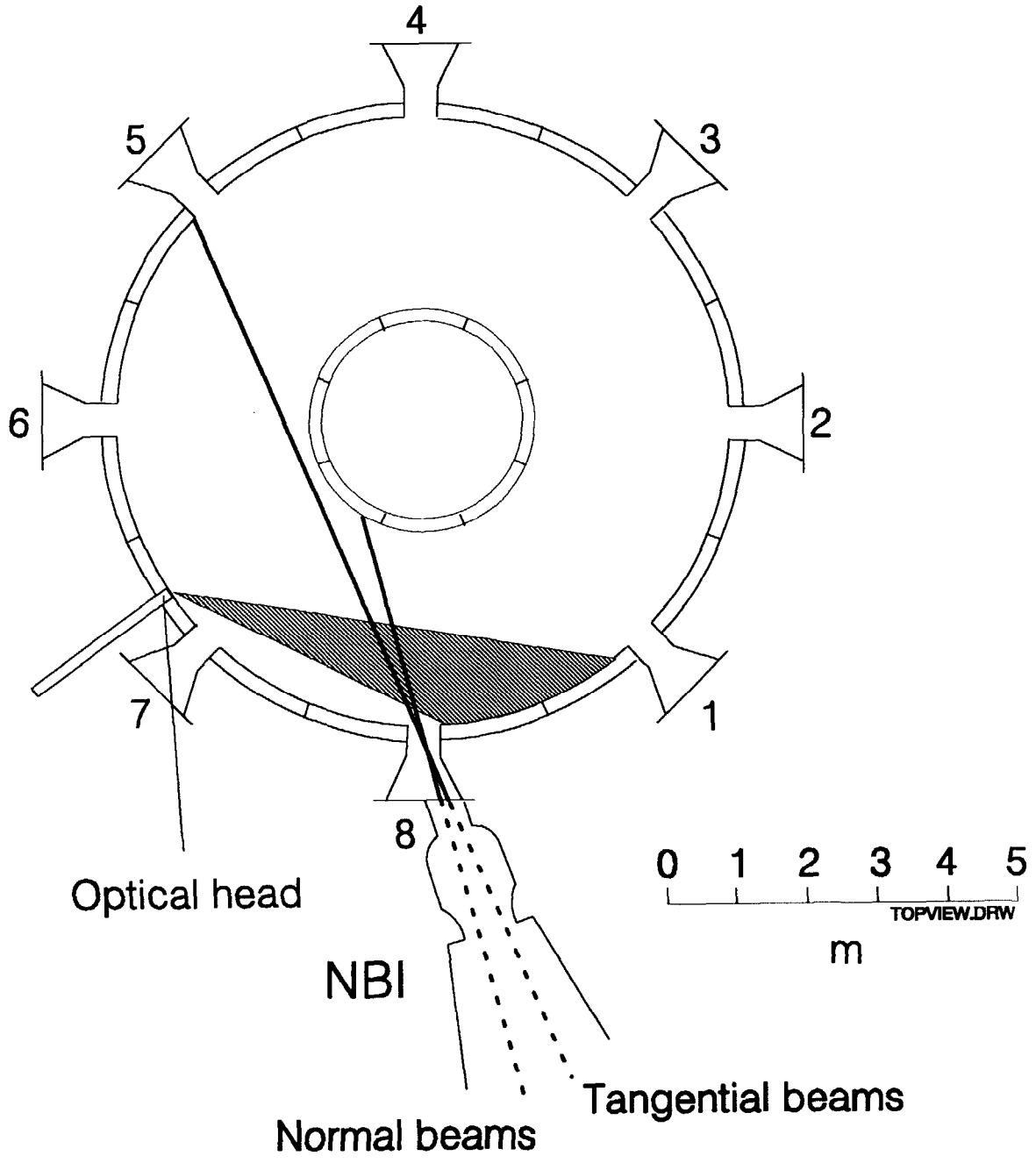

Fig. 3. Plan view of JET showing neutral beam injector (NBI) box at octant 8 and relevant lines of sight (at octant 4 a second NBI box is located). In the horizontal direction the plasma reaches from about 2.0 m to 4.0 m. The magnetic axis lies in the vicinity of 3.1 m.

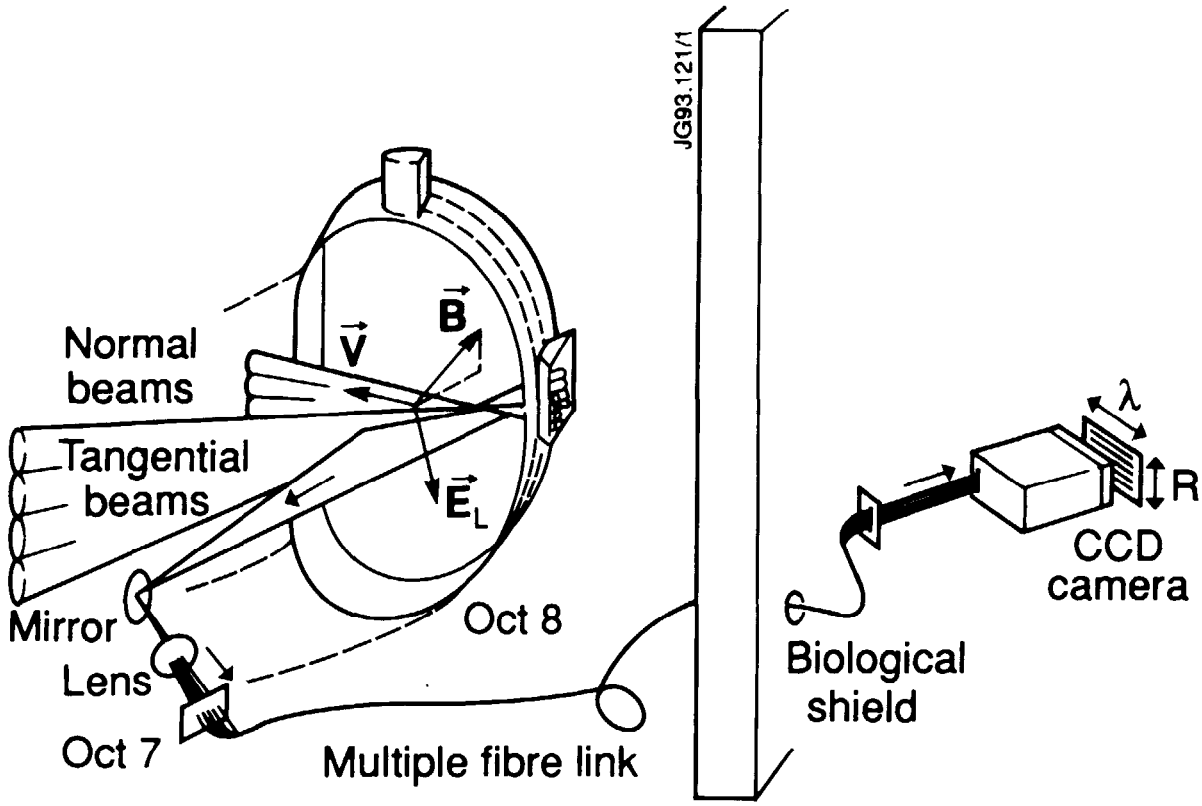

Fig. 4. Overview of the MSE diagnostic. The electric Lorentz field $\vec{E}_L = \vec{v} \times \vec{B}$ is indicated, where $\vec{v}$ is the beam velocity and $\vec{B}$ the total magnetic field. The horizontal dimension of the CCD detector represents the wavelength scale, the vertical dimension the torus major radius.

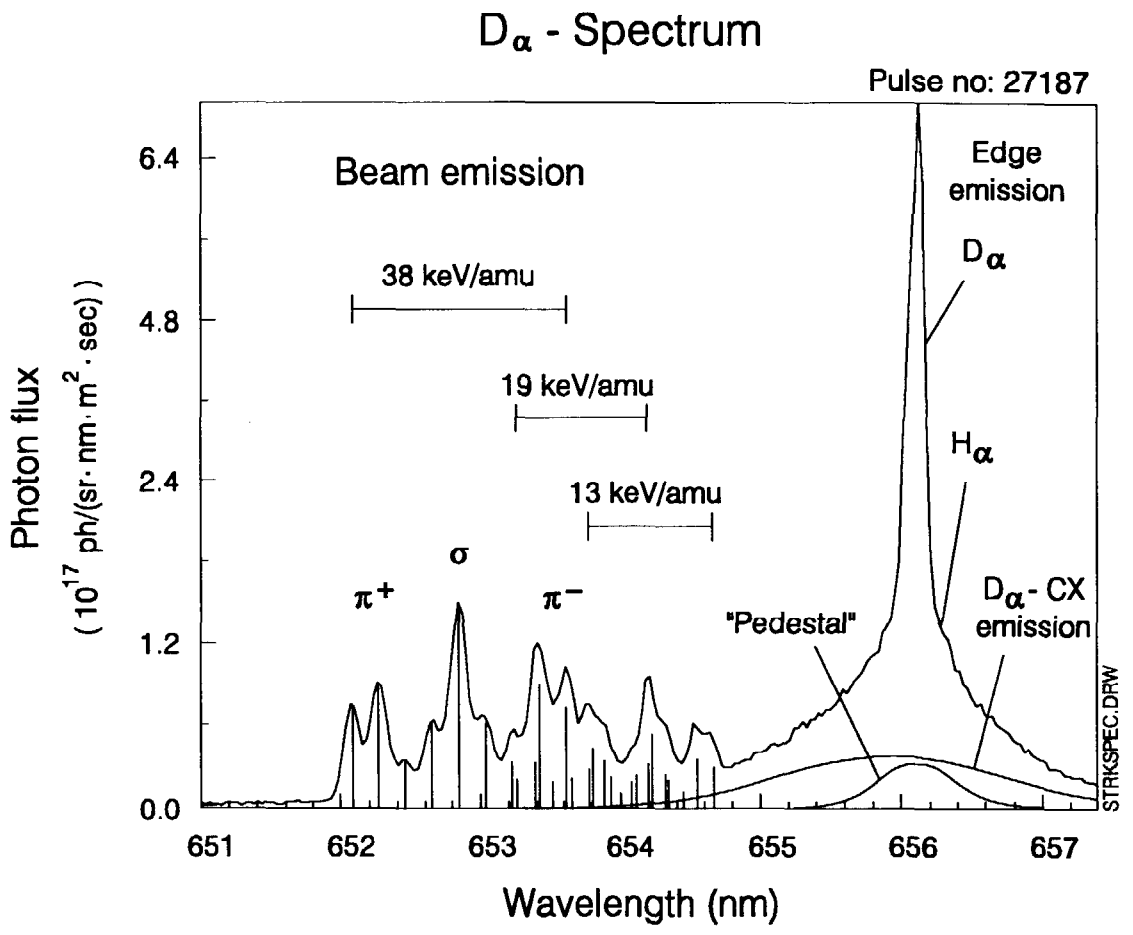

Fig. 5. Spectrum in the vicinity of deuterium Balmer-α with two active neutral beams from the normal bank for a beam energy of 72 keV and a central toroidal magnetic field of 3 T (the amplitudes of the Gauss functions are reduced in scale by a factor of two). σ and π denote the different states of polarization of the BE.

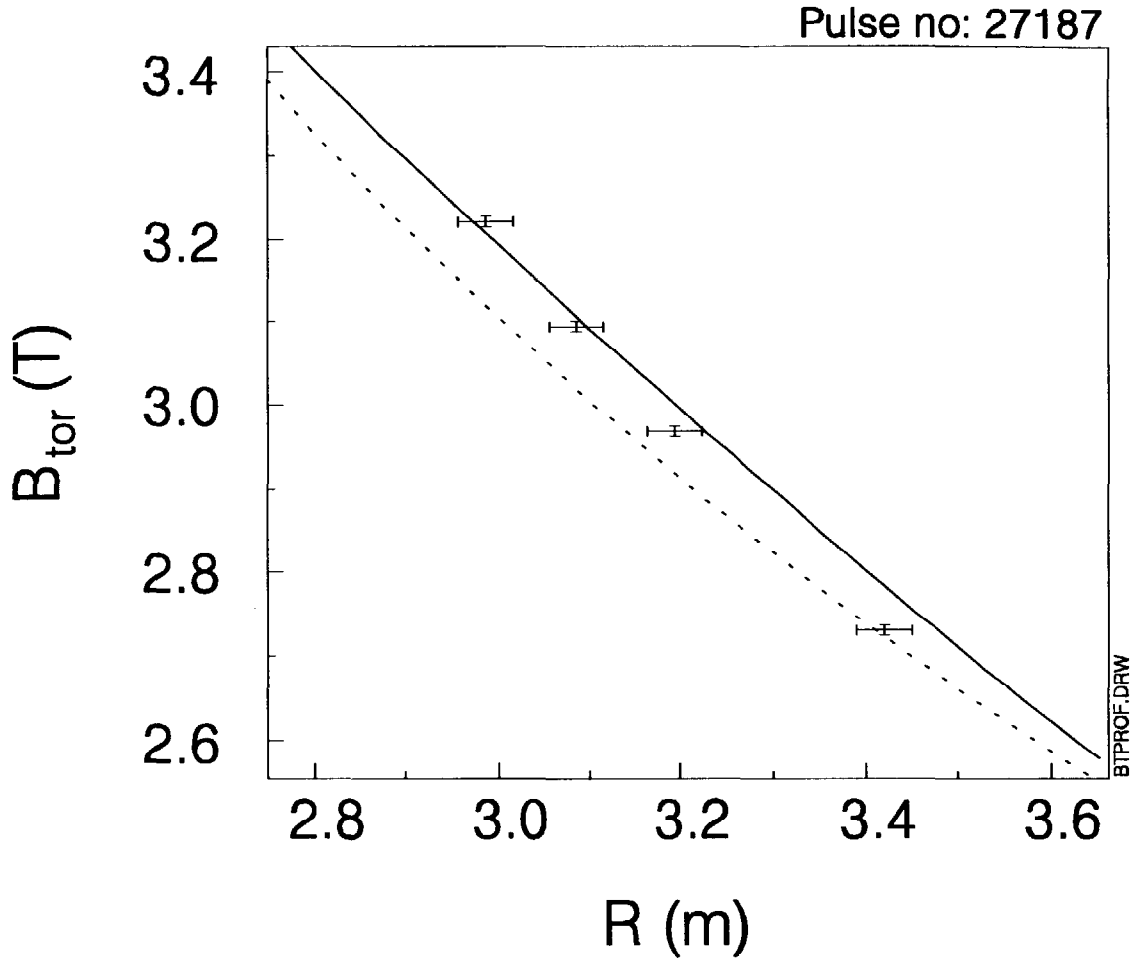

Fig. 6. Comparison of measured toroidal magnetic field with the result from IDENTC (—) and the vacuum B_{tor} (----). The error bars indicate the error of the spectrometer dispersion and an estimate for the radial accuracy of the observation position.

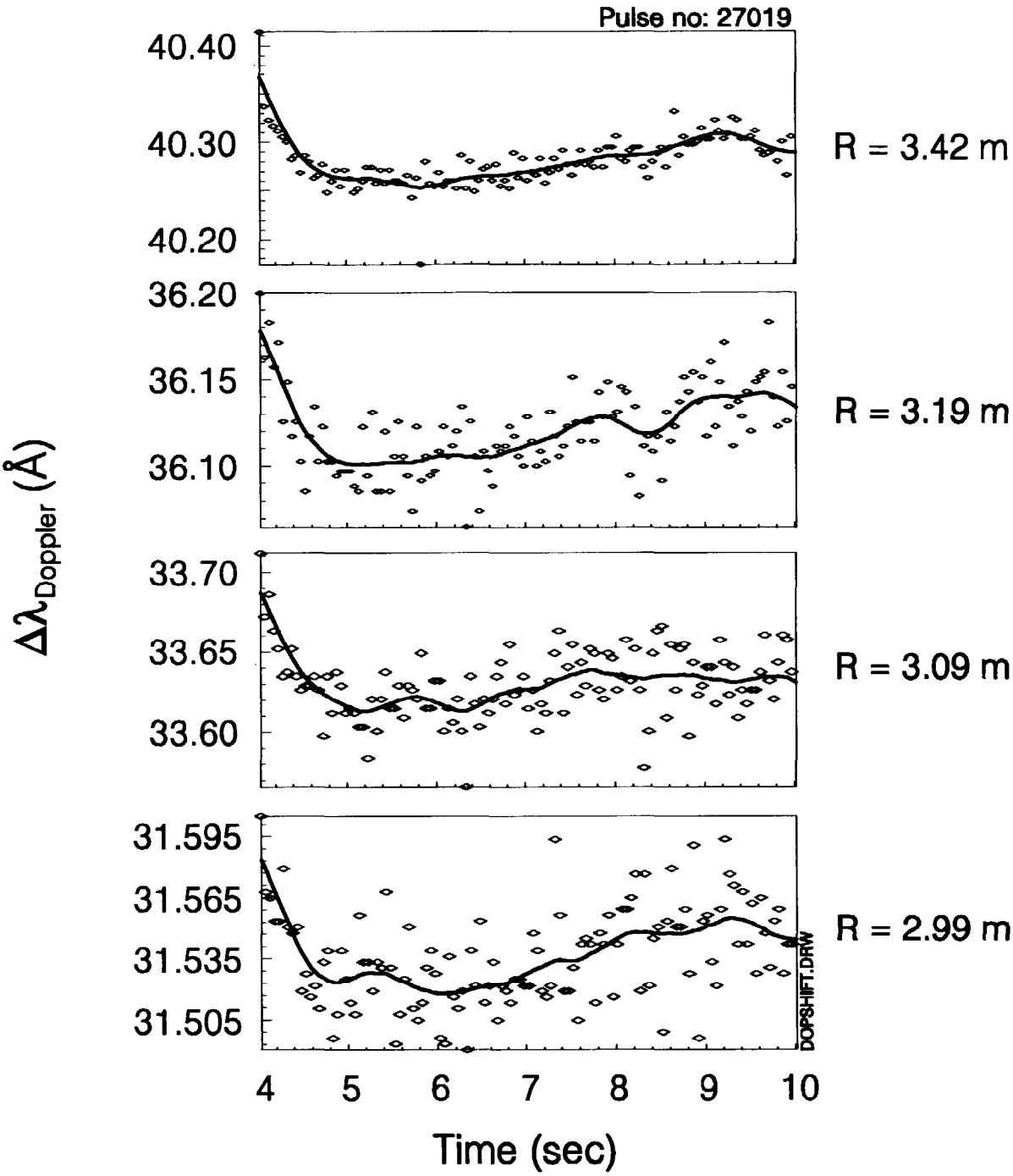

Fig. 7. Evolution of the Doppler shift of the beam emission spectrum. The solid lines represent the data points smoothed with a 1 sec time constant.

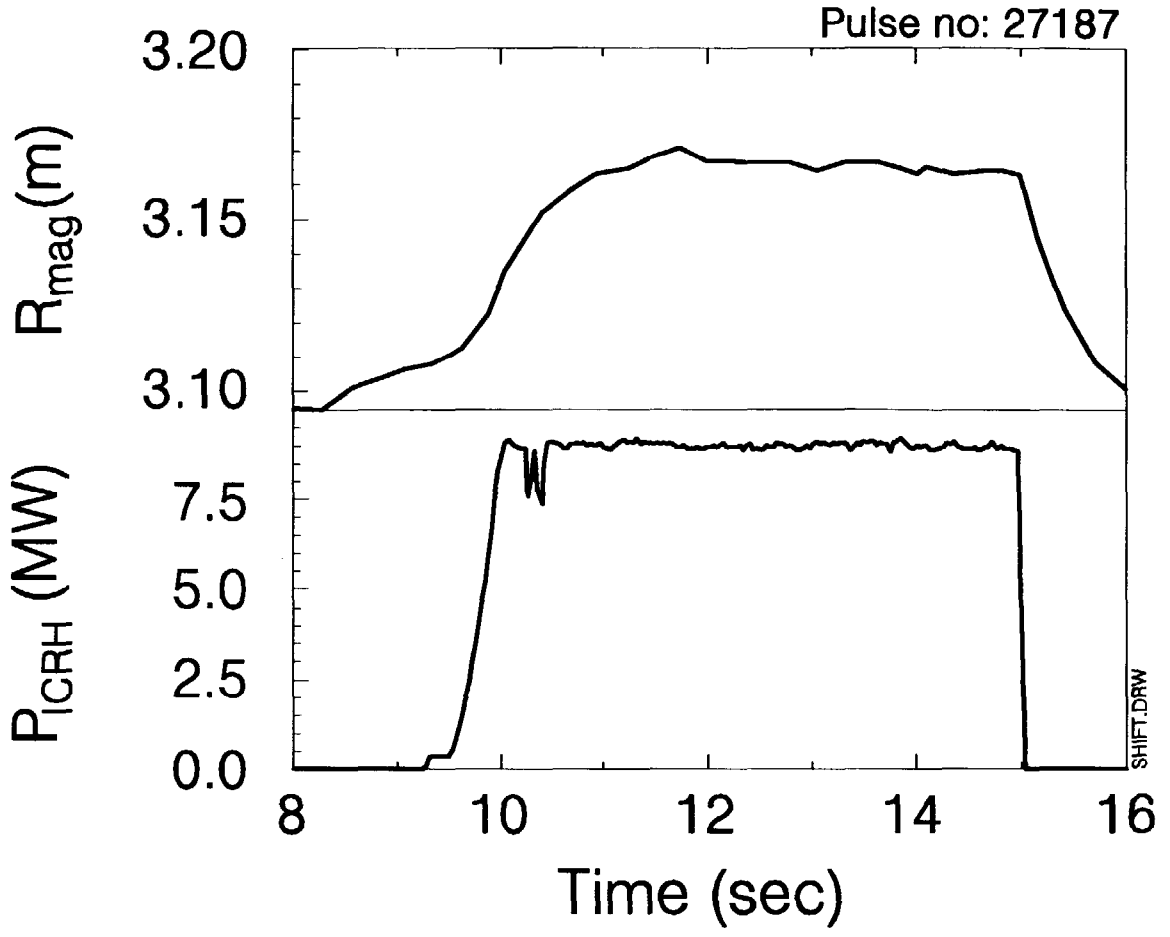

Fig. 8. Shafranov shift of the magnetic axis (R_{mag}) from IDENTC caused by 9 MW of ICRH-power.

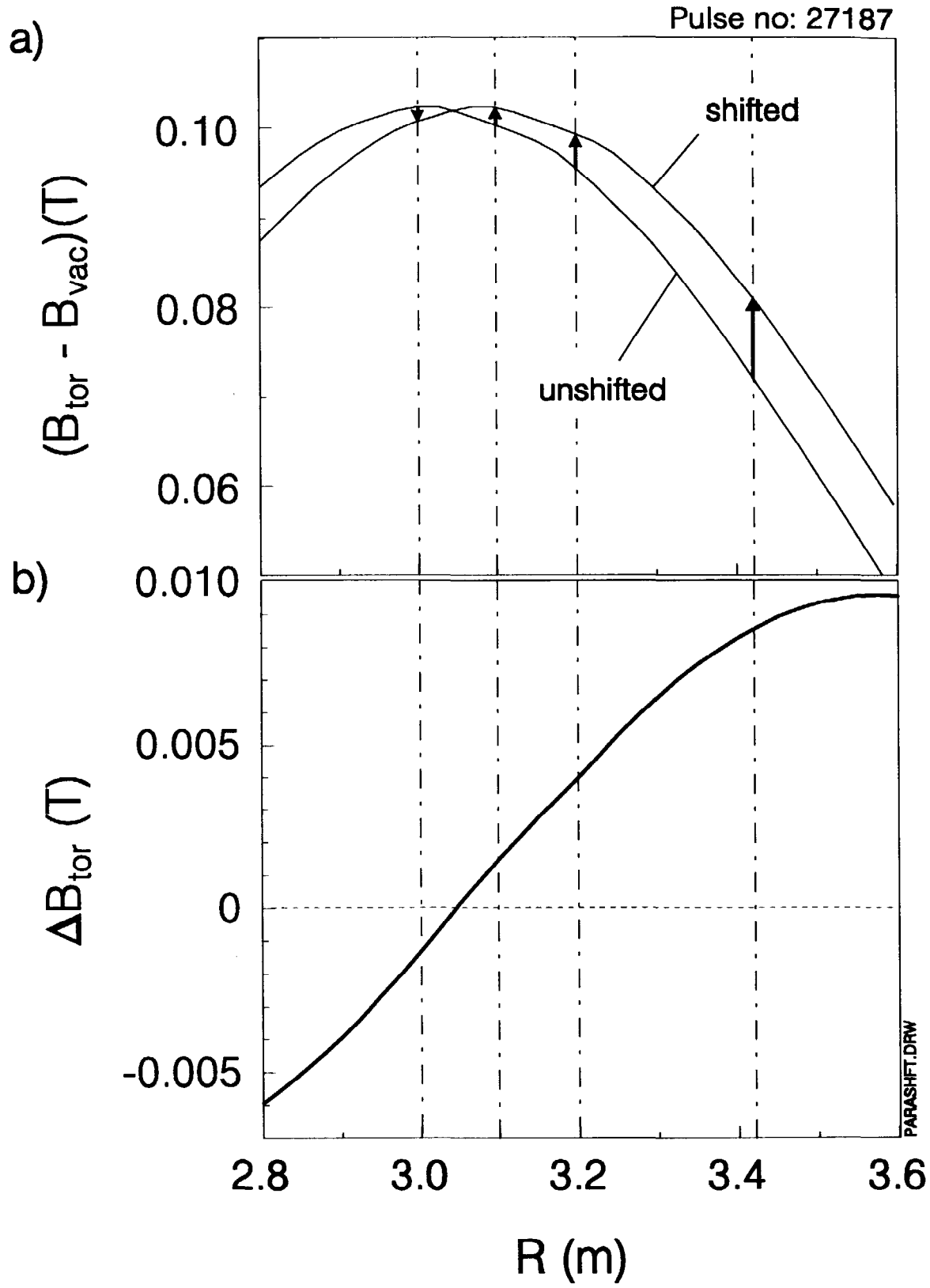

Fig. 9. a) Shift of the paramagnetic correction B_{tor}-B_{vac} (B_{vac}: vacuum magnetic field) due a 7 cm Shafranov shift. b) Resulting change of the local B_{tor}. The observation positions are indicated by dashed lines.

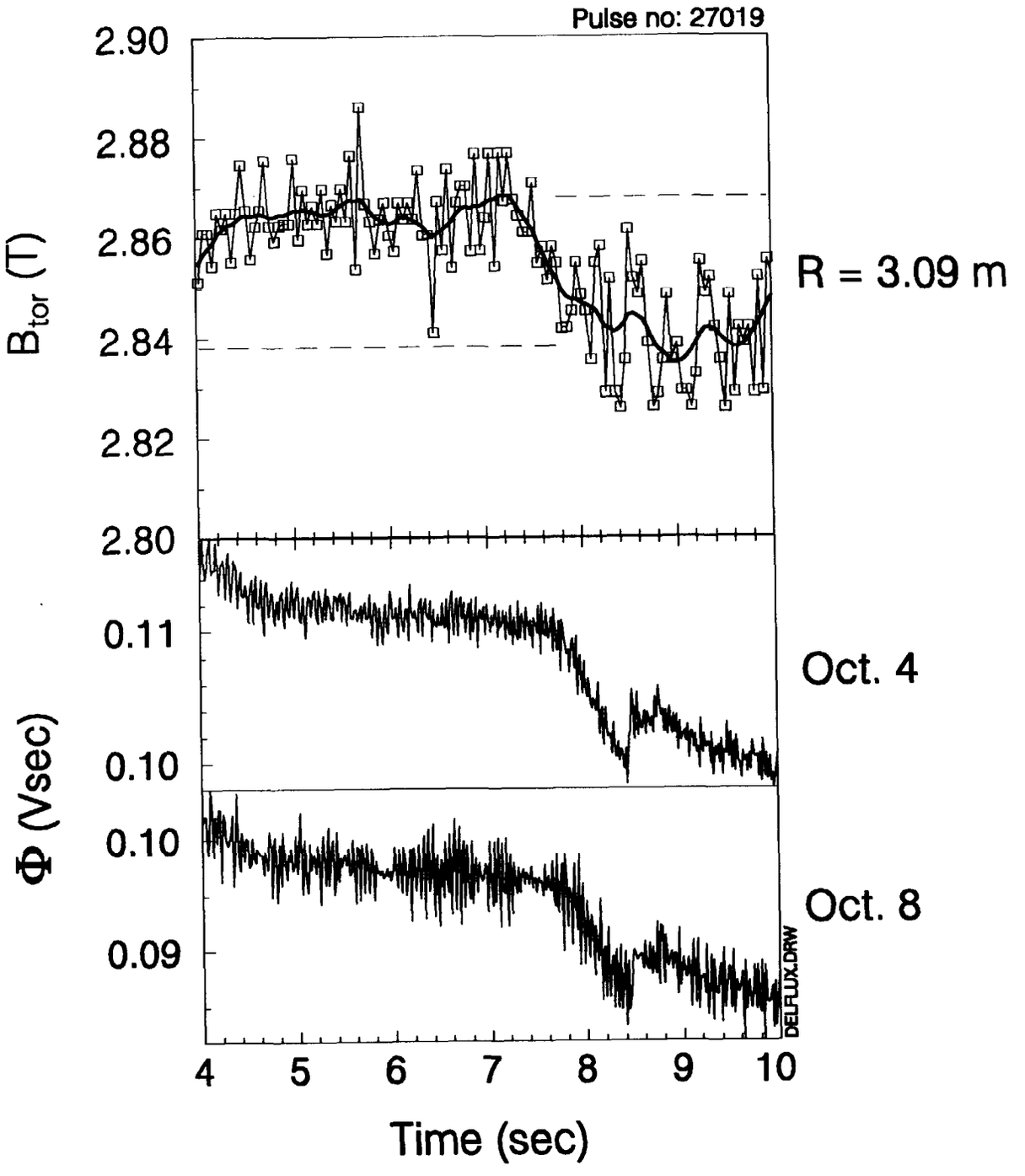

Fig. 10. Comparison of the evolution of the toroidal magnetic field from the MSE measurement with the poloidal flux (Φ) from the diamagnetic loops. Clearly also Φ drops when the B_{tor}-decrease is observed. As the JET plasma is generally paramagnetic, $\Phi > 0$, while the diamagnetism becomes evident in a decrease of Φ.

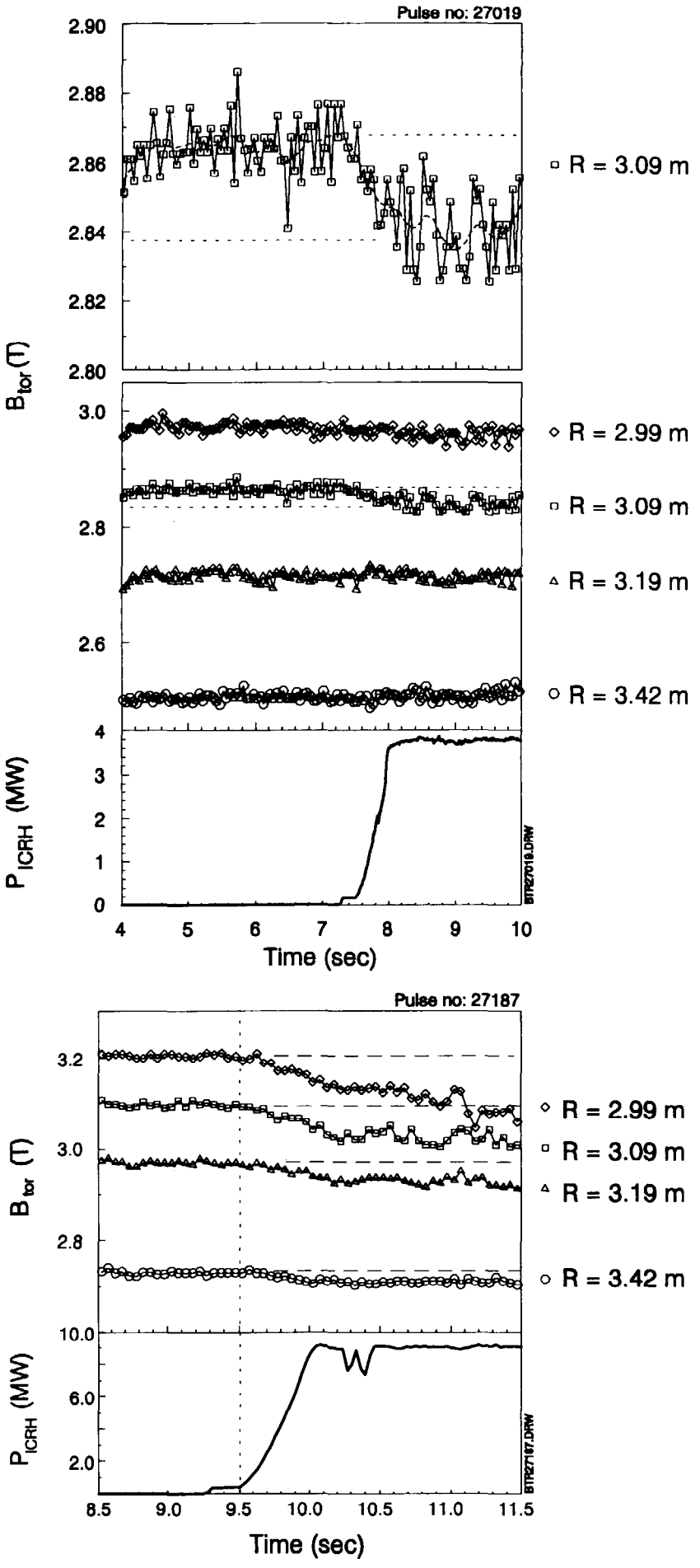

Fig. 11. Time evolution of the measured toroidal magnetic field (B_{tor}) for the available radial positions (R: major radius) in comparison with the total coupled ICRH-power (P_{ICRH}) for two discharges, where P_{ICRH} is substantially different.

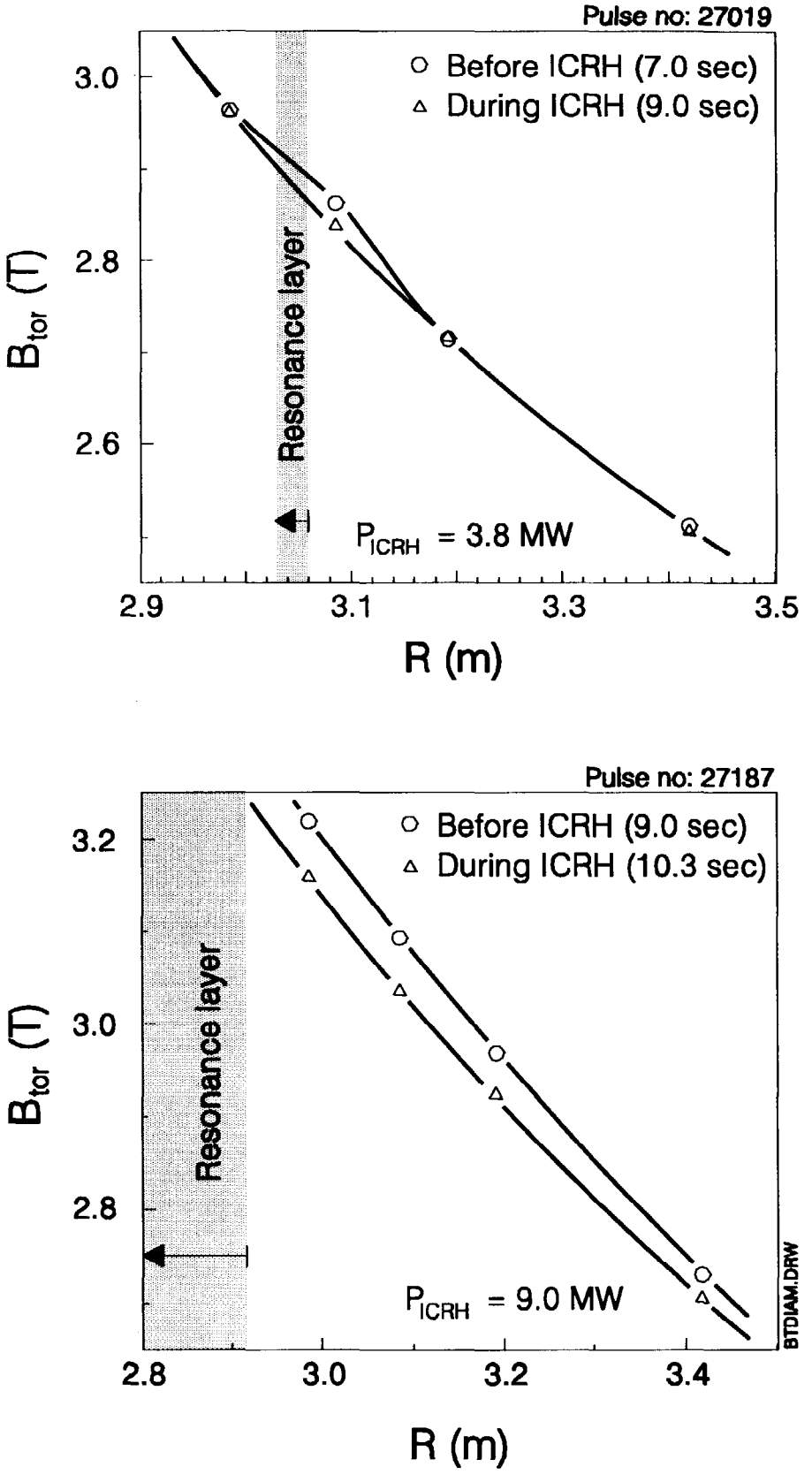

Fig. 12. Toroidal magnetic field vs major radius for time points before and during the ICRH-phase. The shaded regions indicate the position of the RF resonance layer which moves inboard as the toroidal field drops. The error of interest, which is the relative sensitivity of the measurement and is governed by statistical noise only, is in the range of 0.1% - 0.5% (0.003 T - 0.015 T). The absolute error of the profiles lies below 3% (< 0.1 T).

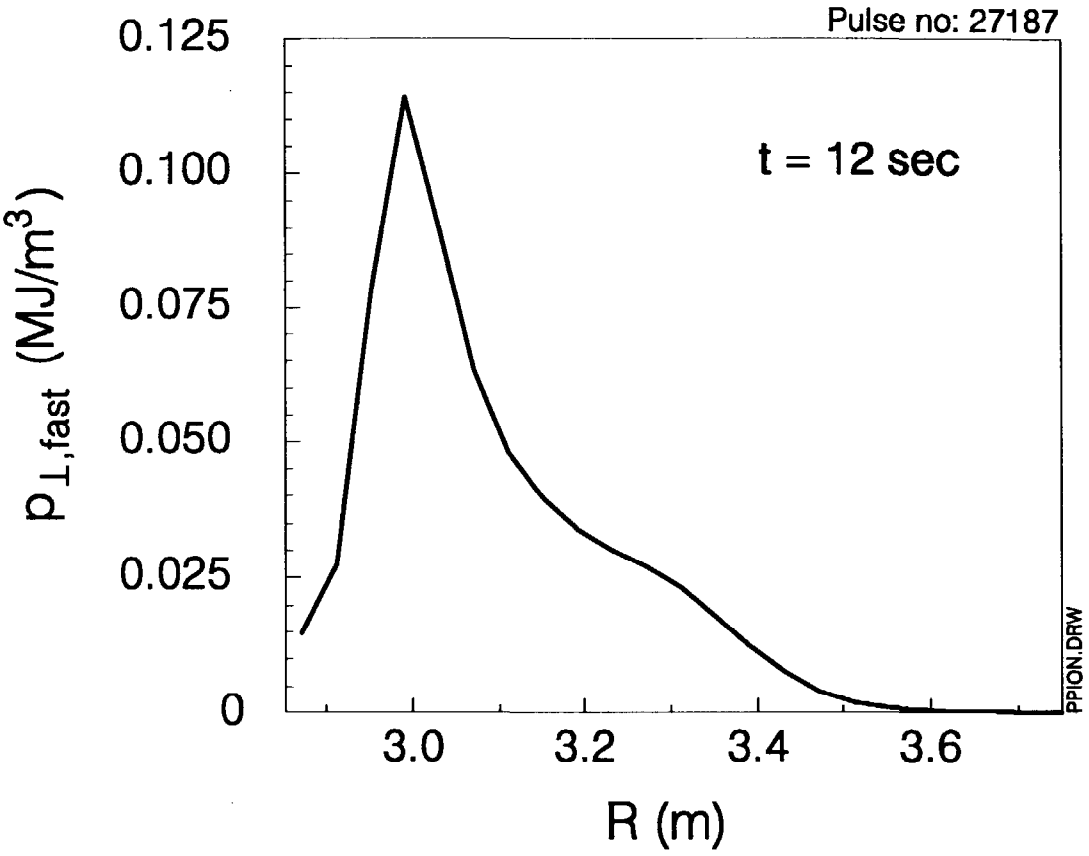

Fig. 13. Profile of the perpendicular fast-ion pressure $p_{\perp,fast}$ calculated by PION-T.

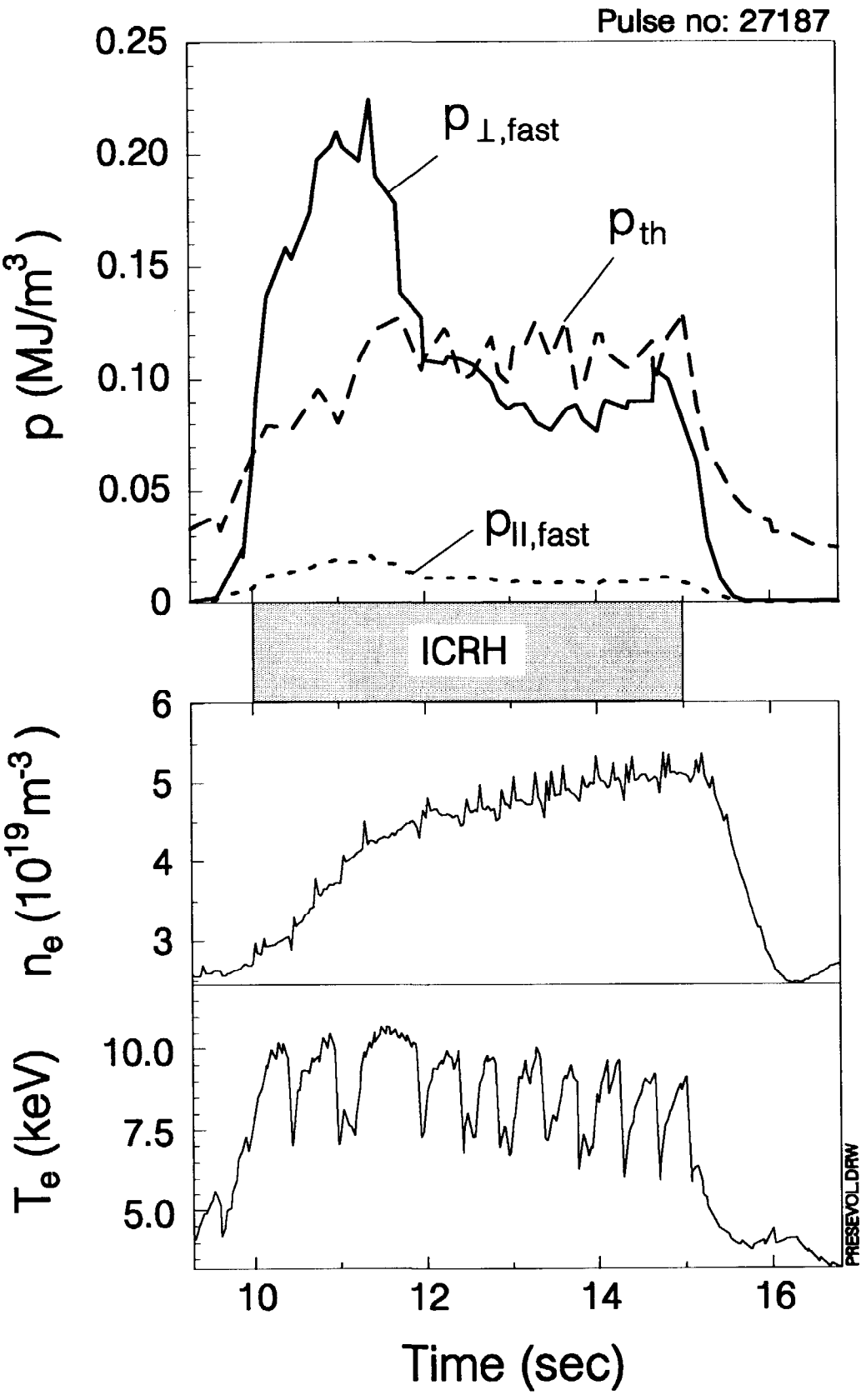

Fig. 14. Maximum parallel and perpendicular fast-ion pressure in comparison with the central electron density and temperature and the resulting thermal pressure.

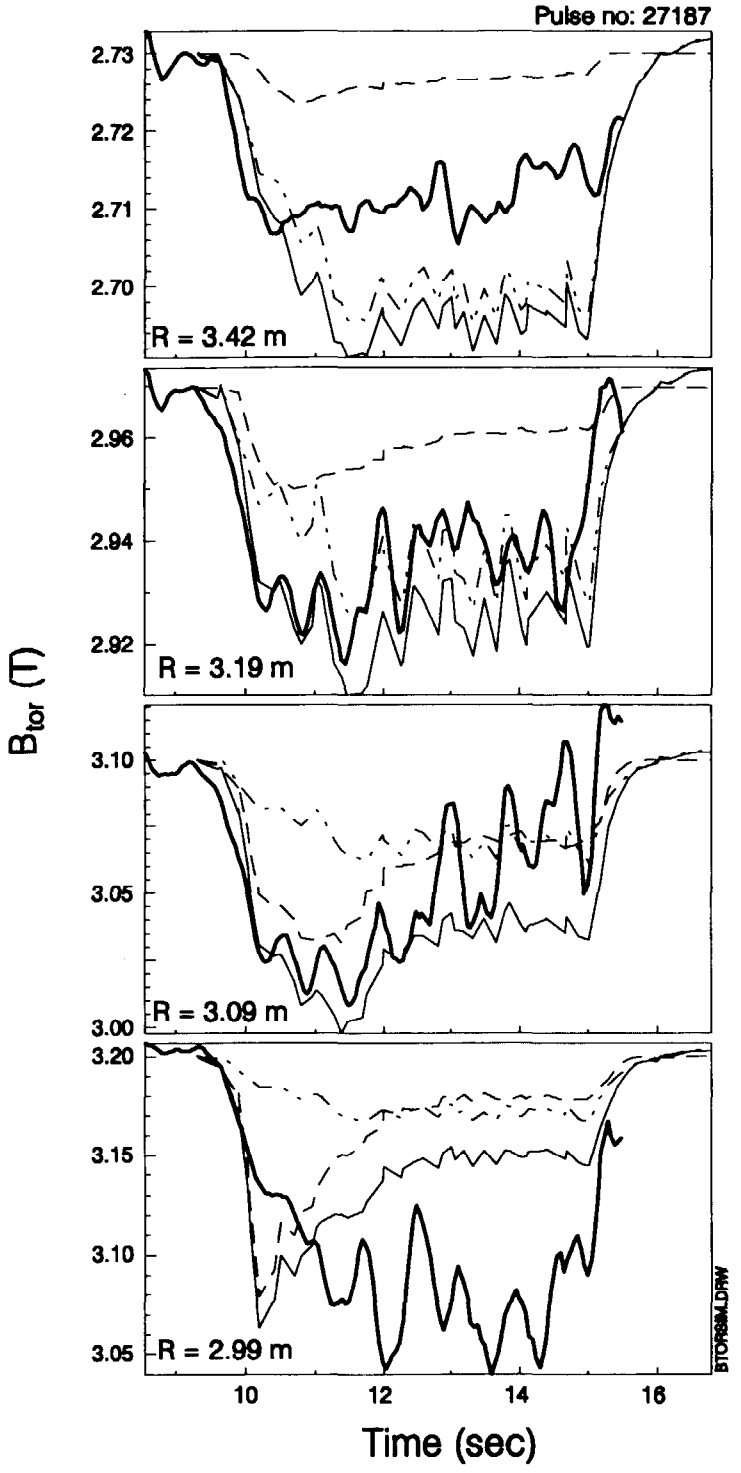

Fig. 15. Evolution of simulated toroidal magnetic field in comparison with the measured field: ——— measured B_{tor},
- - - - - - - simulated B_{tor} inferred from fast-ion pressure,
—·—·— simulated B_{tor} inferred from thermal pressure,
——— total simulated B_{tor}.

The measured data have been smoothed with a 300 msec time constant. It should be noted that individual traces are plotted with different B_{tor}-scales (The B_{tor}-change at 2.99 m is about five times the change at 3.42 m)

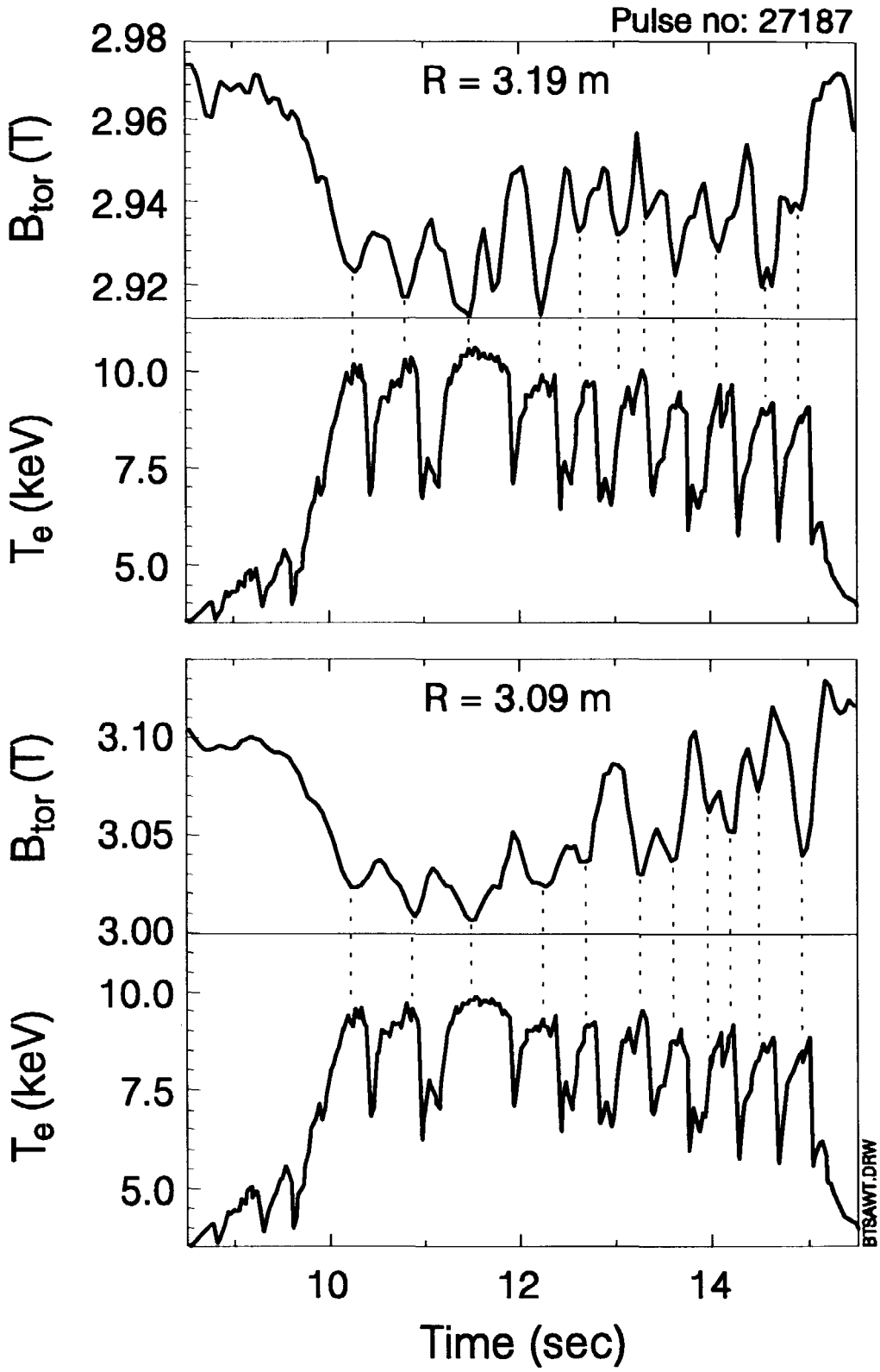

Fig. 16. Correlation between sawtooth oscillations of the electron temperature and the measured toroidal magnetic field (data smoothed with a 100 msec time constant at 3.19 m and 200 msec time constant at 3.09 m).

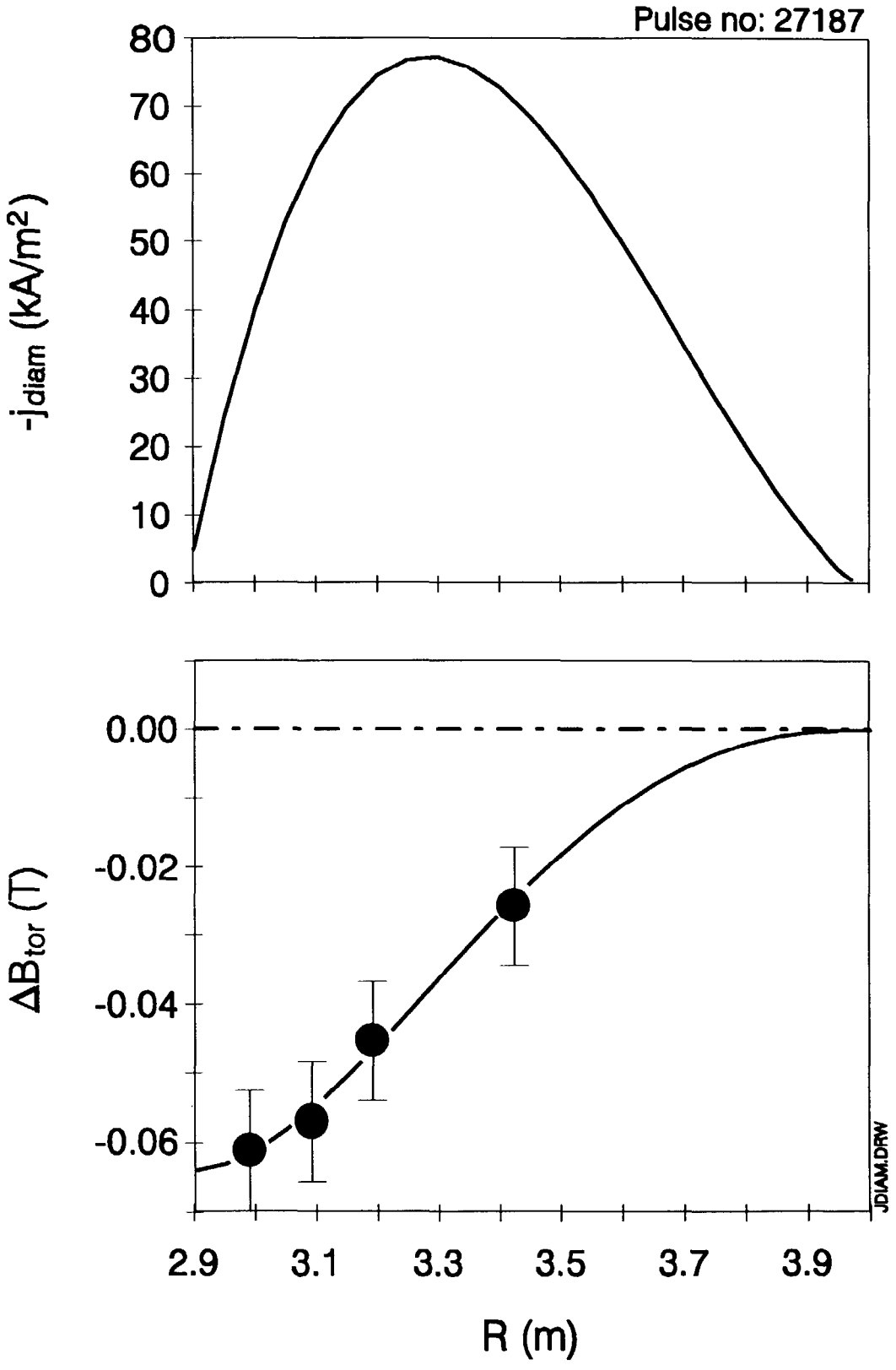

Fig. 17. Diamagnetic current density profile (for convenience $-j_{diam}$ is plotted), which is derived from the change of the toroidal magnetic field.

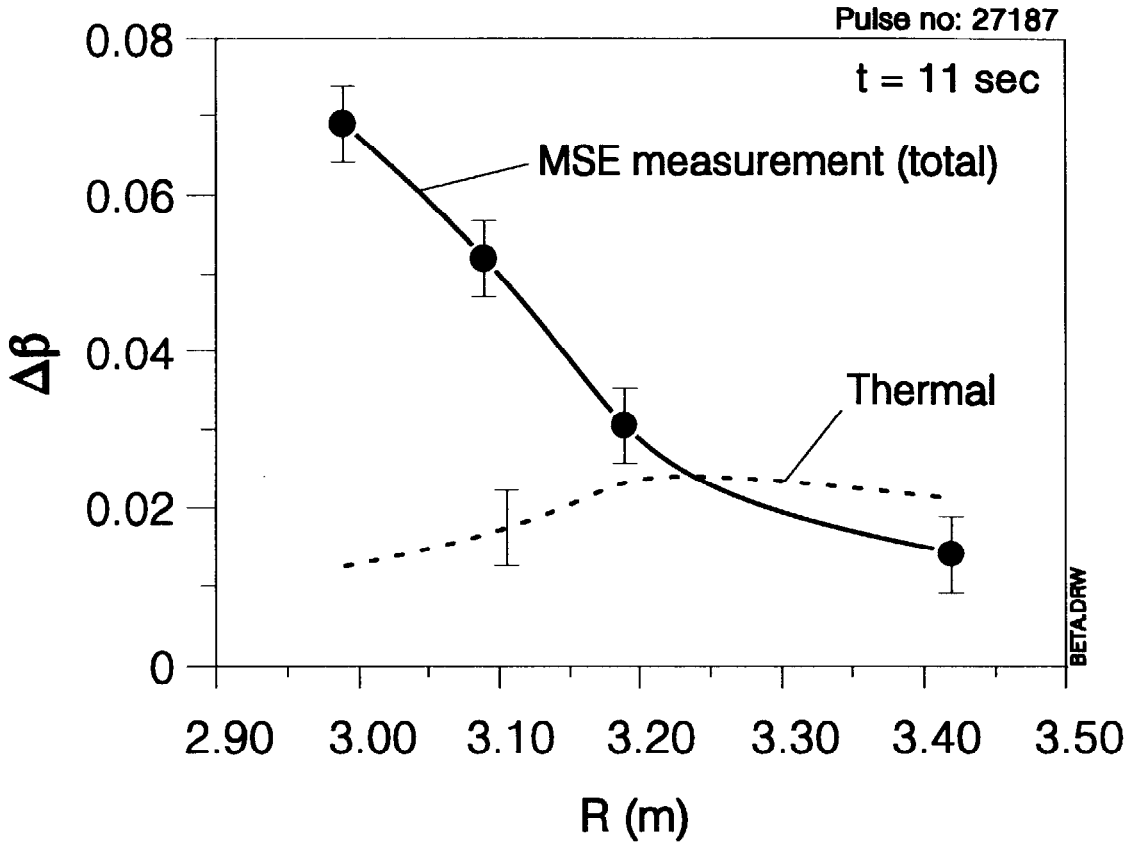

Fig. 18. β-increase due to ICRH. The Δβ inferred from the B_{tor}-decrease is compared with the thermal part inferred from n_e and T_e.